SMALL FORMAT AERIAL PHOTOGRAPHY ACQUISITION OF PARANGTRITIS SAND DUNES AREA USING FIXED-WING UNMANNED AERIAL VEHICLE AND INTEGRATED GROUND CONTROL POINT

Fajrun Wahidil Muharram (1), Farid Ibrahim (1), Nicky Setyawan (2), Putri Meissarah (2), Yuniarsita Setyo Wulandari (1)

[1] Parangtritis Geomaritime Science Park, Kretek, Bantul, DI Yogyakarta, Indonesia
[2] Badan Informasi Geospasial, Cibinong, Bogor, West Java, Indonesia
Email: fajrun.wahidil.m@mail.ugm.ac.id

KEY WORDS: small format aerial photography (SFAP), ground control point (GCP), UAV, sand dunes

ABSTRACT: The condition of sand dunes in Parangtritis coast, Bantul, DI Yogyakarta is getting more critical and endangered. Several pressures of land-use changes such as deforestation, building construction, and illegal mining threaten the existence of this scarce tropical barchan sand dunes. The provision of aerial photography regularly becomes an important thing that must be held to support sand dunes restoration process and decision making by stakeholders. This research aims to provide qualified, rapid, and affordable spatial data usable for high-resolution spatial analysis. Small format aerial photography (SFAP) is commonly used to provide high-resolution spatial data for a limited coverage area. An integration process of ground control point (GCP) towards SFAP is needed to cope with the minimum requirement of accuracy for large scale mapping. SFAP in this research is derived from aerial photography using a fixed-wing unmanned aerial vehicle (UAV) with a Sony Alpha 5000 camera as payload. The payload has 23.2-millimetres x 15.4-millimetres sensor with 20-megapixel resolution and flies in 300-metres altitude above the terrain. The GCP process is conducted by combining two techniques namely premarking and postmarking. The premarking points are distributed in bare land area (sand dunes), while postmarking points are selected among existing objects that can be seen from the aerial photo. The aerial photo generated after the mosaic process has panchromatic wavelength range with 7.5 centimetres spatial resolution and 0.64-metre geometric accuracy using 11 ICPs. It is usable for visual analysis and classification as well as for digital image processing.

1. INTRODUCTION

The condition of sand dunes in Parangtritis coast, Indonesia is getting more critical and endangered (Putra & Harini, 2016). Several pressures of land-use changes such as deforestation, building construction, and illegal mining threaten its existence (Fakhruddin et al., 2010). Geospatial data take an important role in providing geospatial information of such phenomena (Maulana & Wulan, 2015). Thus, its provision is the key to the availability of geospatial data. On the other hand, the use of the unmanned aerial vehicle (UAV) is more common in last decade (James et al., 2017), since its first period for aerial imagery in 1915 (Consortiq, 2020). This equipment has several benefits compared to other kinds of aerial platform, such as more affordable in cost, capable to discover the difficult area, and time-flexible (Stark & Chen, 2014). The provision of aerial photo regularly from UAV becomes an important thing that must be held to support the availability of up-to-date geospatial data of the sand dunes (Maulana & Wulan, 2015), so the effort for restoration process and decision making by stakeholders can be well done. This research aims to provide qualified, rapid, and affordable spatial data usable for high-resolution spatial analysis.

2. MATERIALS

2.1 Research Area

Sand dunes in this research is located in Parangtritis, a village in the south coast of Bantul Regency, DI Yogyakarta Province, Indonesia. The Parangtritis sand dunes is well-known as unique and distinctive tropical coast sand dunes because it has a barchan form. Barchan is one type of sand dunes that is common in an arid area, yet in Parangtritis that has a tropical climate and humid area, barchan can exist (Sugiarto & Sunarto, 2016).

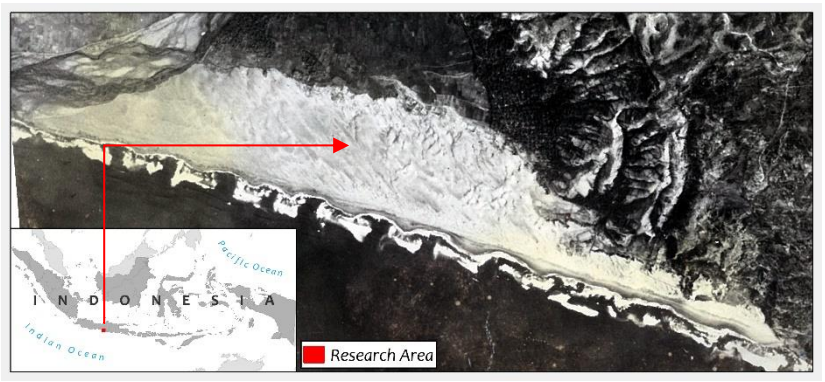

Figure 1. Aerial photo of sand dunes in Parangtritis in 1976

The sand dunes area lies about 412.8 hectares along the coast (Fakultas Geografi UGM, 2015). It borders with a cliff in the east and an estuary of Opak river in the west. An aerial photo of 1976 (Figure 1) shows the virgin condition of the sand dunes that was all covered by bare land. However, now it has been almost covered by other land uses such as vegetation and built area, remaining only 10 hectares (3,7 per cent) of sand coverage.

In 2015, Faculty of Geography of Universitas Gadjah Mada officially recommended the zonation of Parangtritis sand dunes to the Governor of DI Yogyakarta to deal with the effort on the restoration of the sand dunes. Parangtritis Geomaritime Science Park always conducts aerial photography provision as input for this agenda.

2.2 Instruments

Small format aerial photography (SFAP) is commonly used to provide high-resolution spatial data for a limited coverage area (Remondino et al., 2012). An integration process of ground control point (GCP) towards the SFAP is needed to cope with the minimum requirement of accuracy for large-scale mapping (Rangel et al., 2018).

Figure 2. Sky Walker fixed-wing (left) as a platform and Sony A5000 camera (right) as payload

Unmanned Aerial System

The aerial photo is generated using a set of unmanned aerial system that consists of two main parts, airborne segment and ground segment (Sadraey, 2020). The airborne segment includes one unit of unmanned aerial vehicle (UAV) that is Sky Walker fixed-wing craft as the platform, combined with Sony Alpha 5000 camera as payload, flight control system, GNSS device, and 8000mAh battery as the power source (Figure 2). The payload has 16-millimetres focal length and 23.2-millimetres x 15.4-millimetres sensor with 20-megapixel resolution. The ground segment includes telemetry as a signal transmitter, remote control console, and a unit of a computer with Mission Planner © software by ArduPilot.

GNSS Device

The geodetic surveying of GCPs uses Trimble R8s GNSS system. The accurate coordinate value of each point is measured with a geodetic GNSS device using the static method in 10 minutes duration with plotting interval every 15 seconds. The result of the measurement is then corrected using the nearest Continuously Operating Reference Station (CORS) (Rangel et al., 2018), which is located in Parangtritis Geomaritime Science Park belongs to Badan Informasi Geospasial.

3. METHODS

The aerial photo provision is a set of sequential steps. The research framework is illustrated in Figure 3 as follows:

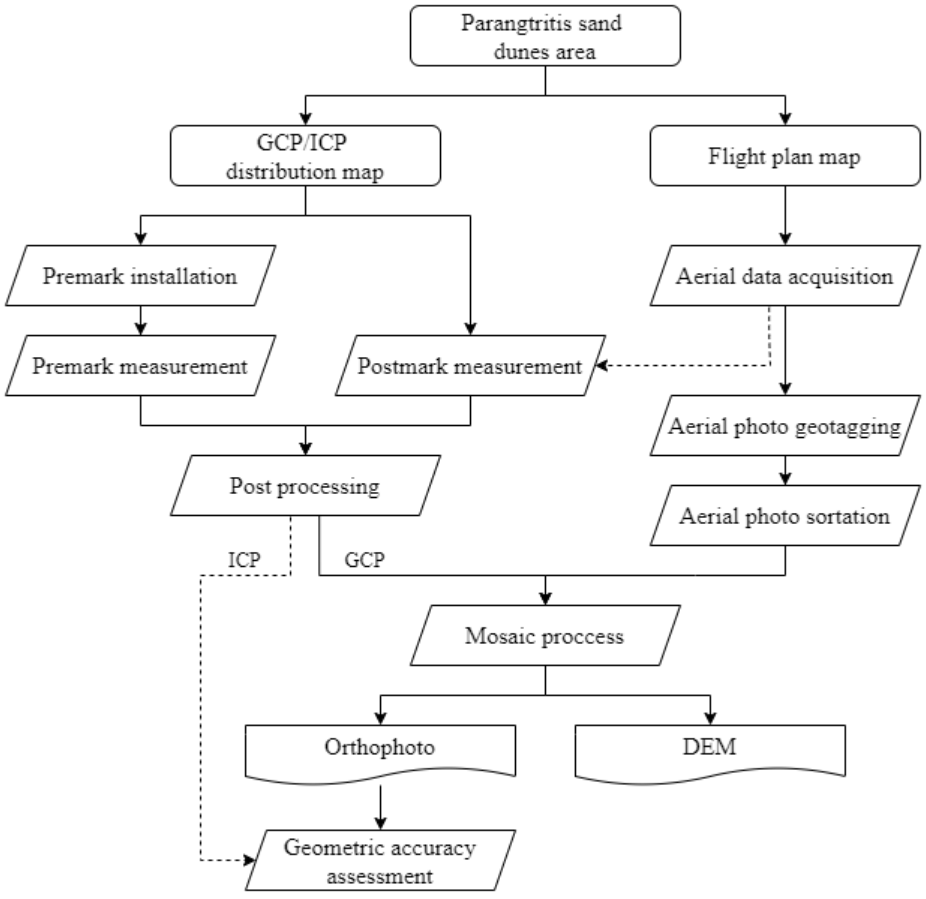

Figure 3. Research framework

3.1 Flight Planning

The area of sand dunes is defined as coverage area that is used to make a flight plan before conducting the aerial data acquisition (Lillesand et al., 2015). This part has some considerations regarding the capability of the UAV to capture photos in one mission such as its maximum flight duration and distance, the end-lap and side-lap of each photo, flight altitude, take-off points (Rangel et al., 2018), as well as the topography and the shape of the sand dunes area. Based on these factors, we used four blocks of flight plan (Figure 4) with flight altitude 300-metres above the terrain.

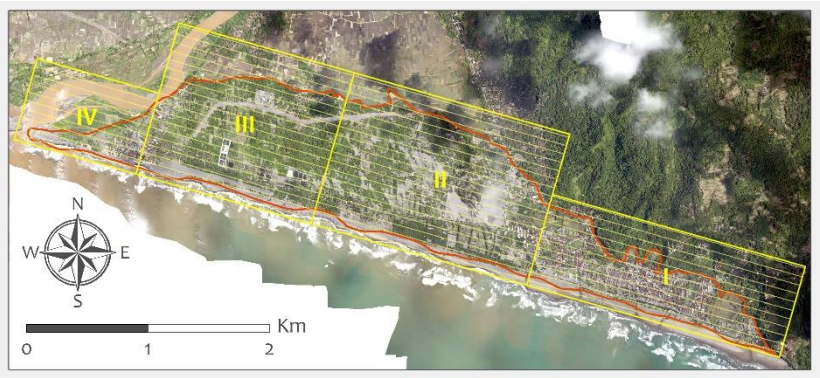

Figure 4. The flight plan of the sand dunes area

3.2 GCP/ICP Distribution

To receive the best result in accuracy, control points are needed to be plotted and should be well distributed in the whole area (Villanueva & Blanco, 2019). These control points are divided into ground control point (GCP) and independent check point (ICP). GCP is used in the mosaic process to improve coordinate value, while ICP is used to measure the accuracy of the aerial photo result (Handayani et al., 2017).

These control points' plotting combines two techniques namely premarking and postmarking (Figure 5). Premark is an artificial X-shaped point that is made from tarpaulin fabric. It is distributed in bare land (sand dunes) area that has no mark to identify in the aerial photo and should have contrast colour towards the environment (Riadi et al., 2018). We use orange or blue colour with the size of 40-centimetres wide and 4-metres long.

Figure 5. Premark (left) that is placed in bare land area (sand dunes) and postmark (right) uses existing clear object

Meanwhile, the postmark is an existing object in the environment and can be clearly identified from the aerial photo (Hackeloeer et al., 2014). Postmark should be a sharp-angled object, contrast towards the environment, low altitude (up to 2 metres above the terrain), and preferably

man-made object such as the edge of a paved field, concrete road, concrete pillar, etc. There are 26 control points (Figure 6) across the coverage area, which consist of 12 premarks and 14 postmarks.

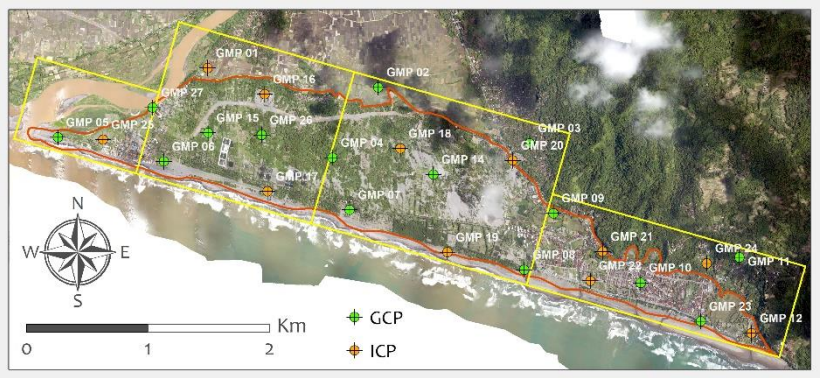

Figure 6. GCP/ICP distribution across sand dunes area

3.3 Aerial Photography Acquisition

Aerial photography acquisition is conducted by considering some factors such as weather condition in term of wind speed, wind direction, rainfall, sun azimuth (McKenna et al., 2017), as well as flight clearance from the authority due to airspace above the sand dunes is a part of flight training area for Indonesian Airforce. The ground control station is chosen in the nearest wide area for take-off and landing and optimum coverage for flight and signal transmission between the aircraft and flight control in the ground (Anas, 2013).

Figure 7. Flight plan while conducting aerial photo acquisition

3.4 Aerial Photo Geotagging and Quality Control

Aerial photo geotagging as post-acquisition process is performed by injecting GPS log file into each aerial photo using the same software as the flight plan, thus each photo has XYZ coordinates from built-in GNSS in the platform. Manual quality control is then conducted to exclude unqualified photos for the next process (Rangel et al., 2018). From 649 photos acquired (Table 1) , there are 6, 2, 6, and 1 photos from flight I, II, III, and IV respectively which were excluded for further process such as high oblique photo, non-aerial photo, and wrong coordinate photo.

Table 1. Numbers of photos per flight

Flight number	**I**	**II**	**III**	**IV**
Number of photos	161	216	205	67
Photos used in the mosaic process	155	214	199	66

3.5 Photo Mosaicking

The rest of all GPS-tagged photo is then mosaiced through Agisoft Metashape © software, using several default steps including Align Photo, Import Reference, Build Dense Cloud, Build Mesh, Build Texture, Build Tiled Model, Build DEM, and Build Orthomosaic (Table 2). Import reference is a step where all the GCPs are added to the mosaic process. This process ends with Orthomosaic and DEM data export, resulting in two outputs that is orthophoto and digital surface model of the sand dunes.

Table 2. The input, parameters, and output in the processing workflow

Workflow step	**Metashape parameters**	
General	Cameras: 637	Markers (GCPs): 14
	Aligned cameras: 634	
Photo alignment	Points: 590,755 of 628,322	Pair selection: reference
	Accuracy: medium	
Camera optimization	Fit: f, b1, b2, cx, cy, k1-k3, p1, p2	
Depth maps	Counts: 632	Depth filtering mode: aggressive
	Quality: medium	
Dense cloud	Points: 106,580,248	Depth filtering mode: aggressive
	Quality: medium	
Tiled model	Quality: medium	Tile size: 256
	Depth filtering mode: aggressive	Face count: low
	Reconstruction source: dense cloud	
DEM	Size: 28,505 x 16,082	Interpolation: enabled
	Source data: dense cloud	Resolution: 30.1 cm/pixel
Orthomosaic	Size: 91,229 x 45,017	Surface: DEM
	Blending mode: mosaic	Resolution: 7.52 cm/pixel

3.6 Geometric accuracy assessment

The geometric accuracy assessment is conducted towards the orthophoto using ICPs to generate the accuracy of the data result (Padró et al., 2019). This consists of two kinds of assessment, horizontal accuracy as well as vertical accuracy.

The circular error value used is 90 (CE90), which is obtained by formulas as follow:

$$CE90 = 1.5175 \times RMSE_r \quad \text{..... (1)}$$

(SNI 8202:2019 Ketelitian Peta Dasar, 2019)

$$RMSE_r = \sqrt{\sum_{n=1}^{n} \frac{(X_{ground_i} - X_{data_i})^2 + (Y_{ground_i} - Y_{data_i})^2}{n}} \quad \text{..... (2)}$$

(Villanueva & Blanco, 2019)

While the linear error value used is 90 (LE90), which is obtained by formulas as follow:

$$LE90 = 1.6499 \times RMSE_z \quad \text{..... (3)}$$

(SNI 8202:2019 Ketelitian Peta Dasar, 2019)

$$\mathrm{RMSE_z} = \sqrt{\sum_{n=1}^{n} \frac{(\mathrm{Z}_{ground_i} - \mathrm{Z}_{data_i})^2}{n}} \quad \text{..... (4)}$$

(Villanueva & Blanco, 2019)

$\mathrm{RMSE_r}$: root mean square error for x and y position (horizontal)
$\mathrm{RMSE_z}$: root mean square error for z position (vertical)
n : number of samples
x : coordinate point of X-axis
y : coordinate point of Y-axis
z : coordinate point of Z-axis

4. RESULT AND DISCUSSION

4.1 SFAP Output

The aerial photo acquisition was conducted in three days on August 14—16, 2019 during the dry season, so the weather condition deals with the research. The time of acquisition was around 9am—10am (Table 3), considering to receive optimum sun azimuth and sun elevation, as well as the minimum shadow of a cloud. It resulted in 634 single photos with the actual end-lap of 75 per cent and side-lap of 41 per cent.

Table 3. Aerial photo acquisition date, time, sun azimuth, sun elevation, and coverage area

Flight number	**I**	**II**	**III**	**IV**
Acquisition date	08/14/2019	08/14/2019	08/16/2019	08/15/2019
Local time interval	09:37 → 10:16	08:56 → 09:17	08:32 → 09:17	09:46 → 09:54
Sun azimuth interval	64.69 → 55.44	66.95 → 64.69	69.74 → 65.38	61.15 → 59.88
Sun elevation interval	38.12 → 50.82	33.38 → 38.12	28.15 → 38.44	44.69 → 46.41
Coverage area (ha)	167.8	238.6	193.9	72.2

The aerial photo generated after mosaic has panchromatic wavelength range with 7.5 centimetres spatial resolution (Figure 8), while the DEM as secondary out has 30.1 centimetres spatial resolution (Figure 9).

Figure 8. Small format aerial photo derived from UAV acquisition after the mosaic process

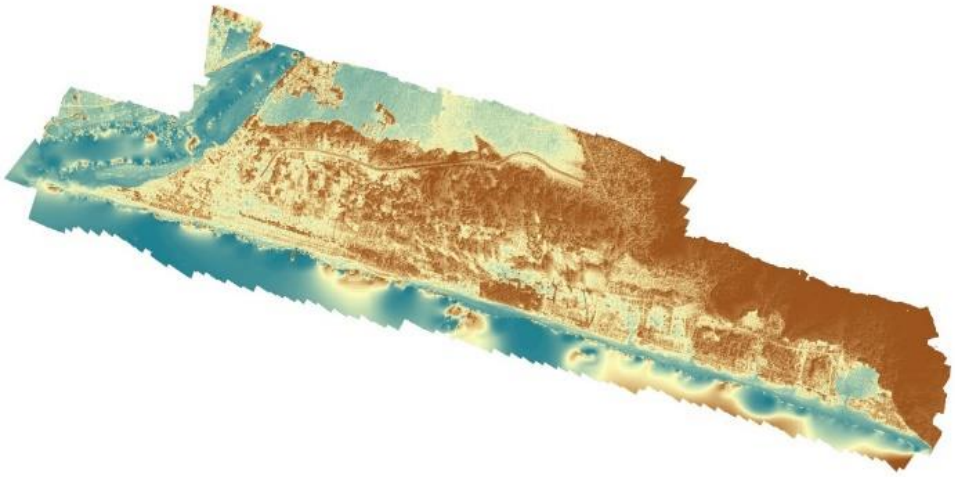

Figure 9. Digital surface model as secondary output from UAV acquisition

4.2 Geometric Accuracy

By using equation (1) and (2), the horizontal geometric accuracy generated from orthophoto is 0.644 metres using 11 ICPs, (Table 4). The horizontal residual (ΔXY) value varies from 0.094—0.778 metres with the $RMSE_r$ of 0.425 metres. The minimum residual is in GMP 24, which is located in the middle of the sand dunes, while the maximum residual is in GMP 17, which is located in the edge of asphalt runway.

Table 4. The result horizontal accuracy using $RMSE_r$ and CE90

Point	X ground	Y ground	X data	Y data	ΔX	ΔY	ΔXY
GMP 25	421782.864	9114283.837	421782.737	9114283.775	-0.540	0.340	0.638
GMP 24	426748.943	9113267.135	426749.065	9113267.299	0.041	0.085	0.094
GMP 22	425792.366	9113122.754	425792.385	9113122.760	-0.136	0.253	0.287
GMP 21	425891.539	9113365.077	425891.485	9113364.966	-0.194	-0.053	0.202
GMP 20	425152.099	9114111.965	425152.206	9114111.970	-0.064	-0.275	0.282
GMP 19	424616.340	9113358.850	424616.649	9113358.047	0.076	-0.439	0.446
GMP 18	424228.595	9114210.105	424229.151	9114210.087	0.320	-0.146	0.352
GMP 17	423133.927	9113859.440	423134.954	9113858.728	0.700	-0.340	0.778
GMP 16	423111.488	9114655.774	423112.017	9114656.397	0.225	0.454	0.507
GMP 01	422641.914	9114872.587	422641.934	9114872.676	-0.312	-0.117	0.333
GMP 12	427116.939	9112693.216	427116.894	9112693.226	-0.116	0.238	0.264
						$RMSE_r$	0.425
						CE90	0.644

Meanwhile, by using equation (3) and (4), the vertical accuracy acquired from DEM is 0.984 metre using the same number of ICPs (Table 5). The vertical residual varies from 0.064—1.421 metres with the $RMSE_r$ of 0.596 metres. The minimum residual is in GMP 21, which is located in the edge of the sand dunes, while the maximum residual is in GMP 16, which is located in the geodetic pillar of Parangtritis Geomaritime Science Park.

Table 5. The result vertical accuracy using $RMSE_z$ and LE90

Point	Z ground	Z data	ΔZ
GMP 25	5.695	5.923	0.228
GMP 24	44.065	44.348	0.283
GMP 22	9.789	10.239	0.450
GMP 21	10.021	9.957	0.064
GMP 20	11.475	12.019	0.544
GMP 19	4.249	3.543	0.706
GMP 18	19.137	19.263	0.126
GMP 17	6.234	6.770	0.536
GMP 16	8.700	7.279	1.421
GMP 01	4.688	4.074	0.614
GMP 12	8.958	8.682	0.276
		$RMSE_z$	0.596
		LE90	0.984

4.3 Usability of the SFAP for Parangtritis sand dunes

Based on the result of geometric accuracy calculation, the aerial photo can support high-scale 1:5,000 mapping, as the maximum error permitted is 1.5 metre for CE90 level one. Besides, 1 metre is the maximum linear error permitted for LE90 level one for the derivation of 2 metres interval contour data. Thus, the digital elevation model can be used for further analysis in this level of detail (SNI 8202:2019 Ketelitian Peta Dasar, 2019). Moreover, the capability of SFAP to capture in incidental time supports more the provision of geospatial data of the sand dunes of Parangtritis (Maulana & Wulan, 2015). Both visual interpretation and digital image processing are possible to be conducted with this high-resolution aerial imagery and DEM.

5. CONCLUSION

The SFAP generated from this research is usable for high-resolution spatial analysis and classification for both visual interpretation and digital image processing.

ACKNOWLEDGEMENTS

The authors would like to thank Yoniar Hufan Ramadhani and Anggoro Cahyo Fitrianto from Badan Informasi Geospasial and Abdul Majid from AMX UAV Technologies who became pilot and co-pilot, Fredy Satya from Mitra Geotama Indonesia who recommended the flight plan map and GCP map, as well as all interns of Parangtritis Geomaritime Science Park who directly got involved in this project.

REFERENCES

Anas, A. 2013. Sensor Kamera untuk Pemotretan dari Udara Menggunakan UAV. *Media Dirgantara LAPAN*, *8* (2), pp. 2–5.

Badan Standardisasi Nasional. 2019. *SNI 8202:2019 Ketelitian Peta Dasar*. Jakarta.

Consortiq. 2020. *A Short History of Unmanned Aerial Vehicles (UAVs) | Blog | Draganfly*,

Retrieved October 18 2020, from https://consortiq.com/short-history-unmanned-aerial-vehicles-uavs/.

Fakhruddin, M., et al. 2010. Dinamika Pemanfaatan Lahan Bentang Alam Gumuk Pasir Pantai Parangtritis, Kabupaten Bantul. *Jurnal Ilmiah Geomatika*, *16* (2), pp. 43–60.

Fakultas Geografi UGM. 2015. *Laporan Restorasi Kawasan Gumuk Pasir Parangtritis*. Yogyakarta.

Hackeloeer, A., et al. 2014. Georeferencing: a review of methods and applications. *Annals of GIS*, *20* (1), pp. 61–69. https://doi.org/10.1080/19475683.2013.868826

Handayani, W., et al. 2017. Unmanned Aerial Vehicle (UAV) Data Acquisition for Archaeological Site Identification and Mapping. *IOP Conference Series: Earth and Environmental Science*, *98* (1). https://doi.org/10.1088/1755-1315/98/1/012017

James, M. R., et al. 2017. Optimising UAV topographic surveys processed with structure-from-motion: Ground control quality, quantity and bundle adjustment. *Geomorphology*, *280*, pp. 51–66. https://doi.org/10.1016/j.geomorph.2016.11.021

Lillesand, T. M., et al. 2015. *Remote Sensing and Image Interpretation* (7th Ed.). John Wiley & Sons, Inc.

Maulana, E., & Wulan, T. R. 2015. Pemotretan Udara dengan UAV Untuk Mendukung Kegiatan Konservasi Kawasan Gumuk Pasir Parangtritis. *Simposium Nasional Sains Geoinformasi IV*, *September 2016*, pp. 399–407. https://doi.org/10.13140/RG.2.2.13837.13280

McKenna, P., et al. 2017. Measuring fire severity using UAV imagery in semi-arid central Queensland, Australia. *International Journal of Remote Sensing*, *38* (14), pp. 4244–4264. https://doi.org/10.1080/01431161.2017.1317942

Padró, J. C., et al. 2019. Comparison of four UAV georeferencing methods for environmental monitoring purposes focusing on the combined use with airborne and satellite remote sensing platforms. *International Journal of Applied Earth Observation and Geoinformation*, *75*, pp. 130–140. https://doi.org/10.1016/j.jag.2018.10.018

Putra, M. D., & Harini, R. 2016. Nilai Ekonomi Imbuhan Airtanah dari Air Hujan pada Kawasan Bentang Alam Gumuk Pasir Parangtritis. *Jurnal Bumi Indonesia*, *5* (4), pp. 1–11.

Rangel, J. M. G., et al. 2018. The impact of number and spatial distribution of GCPs on the positional accuracy of geospatial products derived from low-cost UASs. *International Journal of Remote Sensing*, *39* (21), pp. 7154–7171. https://doi.org/10.1080/01431161.2018.1515508

Remondino, F., et al. 2012. UAV photogrammetry for mapping and 3D modeling – current status and future perspectives. *ISPRS - International Archives of the Photogrammetry, Remote Sensing and Spatial Information Sciences*, *XXXVIII-1/*(September), pp. 25–31. https://doi.org/10.5194/isprsarchives-XXXVIII-1-C22-25-2011

Riadi, B., L et al. 2018. Vertical accuracy assessment of DSM from TerraSAR-X and DTM from aerial photogrammetry on paddy fields - Karawang, Indonesia. *Advances in Science, Technology and Engineering Systems*, *3* (4), pp. 187–192. https://doi.org/10.25046/aj030416

Sadraey, M. H. 2020. *Design of Unmanned Aerial Systems* (1st Ed.). Wiley.

Stark, B., & Chen, Y. 2014. Optimal collection of high resolution aerial imagery with unmanned aerial systems. *2014 International Conference on Unmanned Aircraft Systems, ICUAS 2014 - Conference Proceedings*, pp. 89–94. https://doi.org/10.1109/ICUAS.2014.6842243

Sugiarto, F., & Sunarto. 2016. Pengaruh Bangunan Terhadap Perkembangan Gumuk Pasir Parangtritis. *Jurnal Bumi Indonesia*, *5* (4), pp. 1–10.

Villanueva, J. K. S., & Blanco, A. C. 2019. Optimization of ground control point (GCP) configuration for unmanned aerial vehicle (UAV) survey using structure from motion (SFM). *ISPRS - International Archives of the Photogrammetry, Remote Sensing and Spatial Information Sciences*, *XLII-4/W12* (4/W12), pp. 167–174. https://doi.org/10.5194/isprs-archives-XLII-4-W12-167-2019